npj | 2D materials and applications

Article

Published in partnership with FCT NOVA with the support of E-MRS

https://doi.org/10.1038/s41699-024-00452-1

Highly sensitive and reversible MXene-based micro quartz tuning fork gas sensors with tunable selectivity

Wei Ding[1,6], Jingjing Yu[1,2,6], Francis Tsow[3], Laxmi Raj Jaishi[1], Buddhi Sagar Lamsal[1], Rick Kittelson[1], Sarwar Ahmed[1], Parashu Kharel[4], Yue Zhou[5] & Xiaojun Xian[1] ✉

Due to their distinctive morphology, significant surface-to-volume ratio, and metal-like electrical conductivity, MXenes have emerged as highly promising gas-sensing materials. Traditional MXene-based gas sensors predominantly rely on the electrical conductivity of MXenes for signal transduction. However, it is crucial to explore alternative signal transduction mechanisms to fully unlock the potential of MXenes in gas sensing applications. In this study, we have successfully showcased the development of a mass-transduction-based MXene gas sensor, utilizing MXenes as the adaptable receptor and MQTF as the transducer. The interaction between the gas analyte and MXenes induces a change in mass, resulting in a resonant frequency shift of the MQTF. This signal transduction mechanism eliminates the dependency on the electrical conductivity of MXenes, offering a broader range of possibilities for chemical modification of MXenes without concerns about compromising their conductivity. By engineering $Ti_3C_2T_x$ surfaces, we have demonstrated high sensitivity and selectivity tuning of MXene-MQTF gas sensors for detecting CO, SO_2, and NH_3. This antisymmetric mass-transduction-based (low-cost, stable, sensitive, and practical tuning fork-based) MXene gas sensor demonstrated exceptional sensing performance, customizable selectivity, and high cost-effectiveness. This study paves the way for designing high-performance MXene-based chemical sensors and expands the scope of potential applications in air quality monitoring, wearable devices, the Internet of Things (IoT), and robotics.

As emerging two-dimensional materials, MXenes have demonstrated attractive potentials in energy conversion and storage[1,2], environmental[3] and biomedical application[4], and sensors[5–9], due to their excellent chemical and physical properties, such as metallic conductivity[10], tunable energy bandgap[11], mechanical flexibility[12], and strong hydrophilicity[13]. MXenes have a general formula of $M_{n+1}X_nT_x$, where M stands for an early transition metal, X is carbon and/or nitrogen, and T_x is the abbreviation of terminal surface functional groups, for example, -O, -OH, or -F[14]. These surface functional groups provide a tremendous amount of chemically active sites for further modification. MXenes have found applications in various sensor types, including but not limited to strain sensors[15], pressure sensors[16], biosensors[17], and gas sensors[18], owing to their distinctive properties.

Because of their unique morphology, large surface-to-volume ratio, and metal-like electrical conductivity, Mxenes have been considered promising gas-sensing materials. MXenes-based gas sensors, such as chemiresistive sensors[19–23], capacitive sensors[24], electrochemical sensors[25–27], and piezo-resistive sensors[28–30] have been reported. These sensors mainly utilize the electrical conductivity of MXenes in their sensor signal transducing mechanism. Exploring other signal transducing mechanisms is crucial to further unleash the potential of MXenes in gas sensing applications. Quantifying gas analyte through mass change could allow further utilization of

[1]Department of Electrical Engineering and Computer Science, Jerome J. Lohr College of Engineering, South Dakota State University, Brookings, SD 57007, USA. [2]College of Ecological Environment and Urban Construction, Fujian University of Technology, Fuzhou, Fujian 350118, China. [3]Center for Bioelectronics and Biosensors, The Bio-design Institute, Arizona State University, Tempe, AZ 85281, USA. [4]Department of Chemistry, Biochemistry and Physics, South Dakota State University, Brookings, SD 57007, USA. [5]Department of Mechanical Engineering, University of Texas at Dallas, Richardson, TX 75080, USA. [6]These authors contributed equally: Wei Ding, Jingjing Yu. ✉e-mail: xiaojun.xian@sdstate.edu

MXenes' surface chemistry to improve the sensor's selectivity without worrying about MXenes' conductivity degradation after chemical modification.

An ideal mass transducer for gas sensing could be the micro-quartz tuning fork (MQTF). MQTF is a piezoelectric quartz-based resonator commonly used as a frequency measurement unit in many digital electronic devices. Among the different types of piezoelectric resonators, MQTF stands out as a highly effective tool due to its exceptional mechanical quality factor (Q)[31]. Compared to other common piezoelectric resonators, the Q factor of MQTF can be much higher, which allows them to be used as a force sensor in atomic force microscopy (AFM) to achieve atomic resolution with ultrahigh sensitivity[32,33]. Moreover, MQTF has low power consumption and small size, making it a preferred sensing unit for the development of wearable and portable devices[34–36]. Other remarkable attributes of MQTF, such as its low cost and stable resonance frequency, also position it as a viable alternative to traditional piezoelectric resonators[37,38]. The operational principle of the MQTF sensor relies on the resonating frequency shift due to the adsorption or desorption of gas molecules on sensing materials coated on its prongs. MQTF's sensing performance depends on two key factors: the quality factor and how the target molecule interacts with the surface of the resonator[39,40]. As the quality factor is an inherent characteristic of MQTF, enhancing sensing performance primarily revolves around altering the interaction between the target gases and the coated sensing materials[41]. Thus, the design of MQTF's surface recognition layer[42] is crucial for high-performance gas sensing.

Gas sensors are essential in air quality monitoring[43], leakage inspection[44], and hazardous chemical detection[45]. Due to rapid economic development, the world continues to grapple with severe air pollution, evident from the escalating presence of harmful and polluting gases in the environment[46]. Among polluting gases, carbon monoxide (CO), sulfur dioxide (SO_2), and ammonia (NH_3) are three important primary gas pollutants[47]. CO is an odorless, colorless, tasteless, and toxic-neutral gas[48], produced by partially oxidized carbon-containing compounds. SO_2 is a major air pollutant with colorless, corrosive, and strong excitant odor[49], generated during industrial operation and coal and oil burning. NH_3 has broad applications in various fields, including biofuels, industrial refrigerants, and textiles[50]. However, it is one of the most harmful alkaline pollutants produced by common industrial production and manufacturing process. Therefore, it is of great interest to develop highly sensitive, selective, and low-cost chemical sensors for CO, SO_2, and NH_3 monitoring.

Herein, we have demonstrated that a mass-transduction-based MXene gas sensor can be created by using MXenes as the tunable receptor and MQTF as the transducer. The binding of the gas analyte to MXenes causes mass change, thus leading to a resonating frequency shift of the MQTF. This signal transducing mechanism does not rely on the electrical conductivity of MXenes, which gives us a wide range of options for choosing the chemical modification of MXenes without worrying about degrading their conductivity. We synthesized $Ti_3C_2T_x$ and introduced different kinds of chemical groups to its surface. By coating surface-modified $Ti_3C_2T_x$ to the tip of MQTF as a recognition layer, MXene-MQTF gas sensors were successfully fabricated for sensitive, selective, and reversible CO, SO_2, and NH_3 detection. Results suggested that compared to pristine $Ti_3C_2T_x$, the surface functionalized $Ti_3C_2T_x$ exhibited a considerably enhanced gas sensing performance due to introducing specific functional groups on the $Ti_3C_2T_x$ surface. Through the surface chemistry engineering of $Ti_3C_2T_x$, the sensitivity and selectivity of MXene-MQTF gas sensors can be tuned. Given the compact dimensions (a few millimeters) and affordable cost (less than $1) of MQTFs, combined with the straightforward sensor fabrication process, MXene-MQTF sensors have the potential to be seamlessly integrated into smart devices as chemical sensing units. Our mass-transduction-based MXene gas sensor demonstrated with high sensing performance, tunable selectivity, and low cost. This study provides a pathway to design high-performance MXene-based chemical sensors. It broadens the potential applications of MXene-based chemical sensors in air quality monitoring, wearable devices, the Internet of Things, and robotics.

Results and discussion

The sensor design and working principle

The schematic diagram and optical image of the tuning fork before and after coating MXene materials are shown in Fig. 1. MQTF has two symmetric prongs. MQTF's surface consists of two regions: metallic film-coated areas, which serve as electrodes for applying an electric field, and bare areas without any metallic film, mainly located at the prongs' tips. The two prongs of the MQTF will oscillate at a specific frequency under applied external AC excitation voltage. The unperturbed resonance frequency (f_0) of the MQTF is affected by the effective

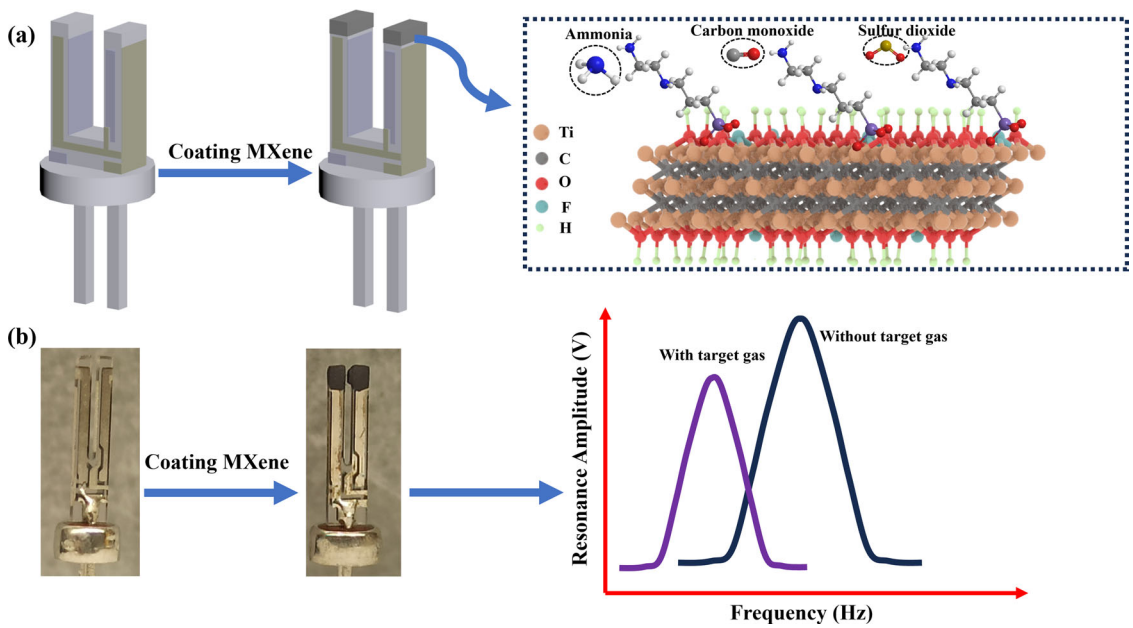

Fig. 1 | Schematic illustration of Mxene-MQTF sensor. a Schematic diagram and **b** optical image of MQTF before and after coating MXene materials.

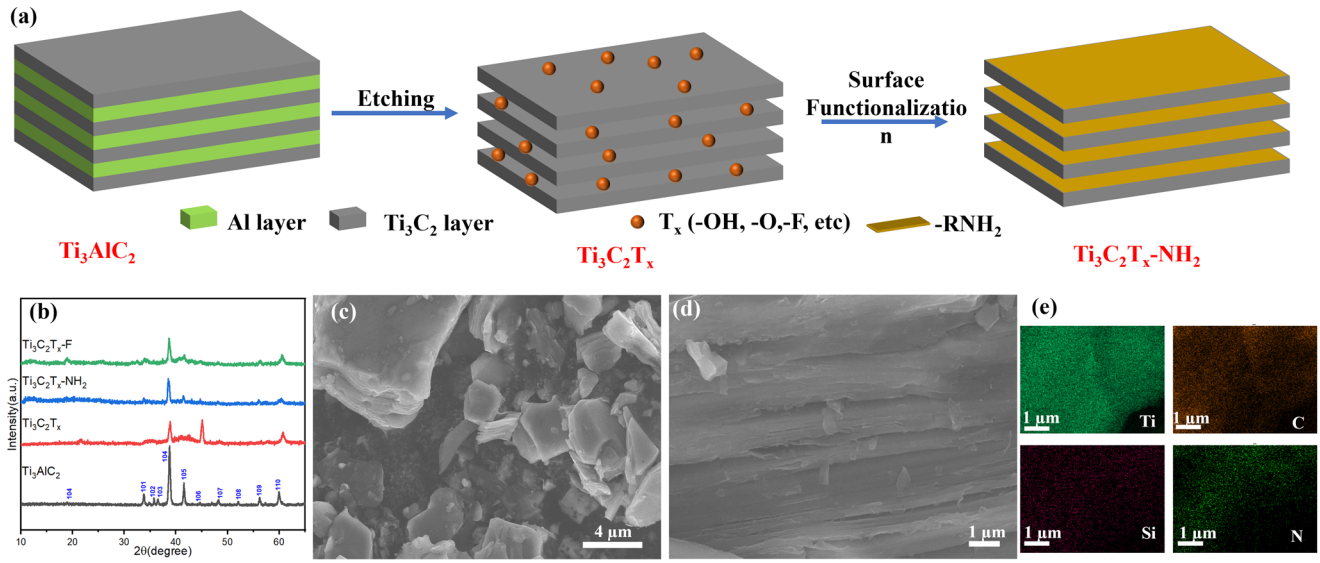

Fig. 2 | Preparation and characterizations of MXene materials. a Schematic illustration of the preparation process for surface functionalized $Ti_3C_2T_x$ -NH_2 sheets. **b** XRD patterns of Ti_3AlC_2, $Ti_3C_2T_x$, $Ti_3C_2T_x$-NH_2 and $Ti_3C_2T_x$-F. **c** Low-resolution and **d** high-resolution SEM images of $Ti_3C_2T_x$-NH_2 powders. **e** The corresponding element mappings of $Ti_3C_2T_x$-NH_2 sheets show a uniform distribution of titanium, carbon, silicon, and nitrogen. Scale bars represent 4 μm in Fig. 2c and 1 μm in Fig. 2d, e.

mass of the MQTF and can be expressed by the following Eq. (1)[34]:

$$f_0 = \frac{1}{2\pi}\sqrt{\frac{K}{m_{\text{eff}}}} \quad (1)$$

Where K is the elastic constant, which is related to the dimension of the oscillation prongs. m_{eff} is the effective mass of the tuning fork.

The MQTF is highly sensitive to mass loading on the prongs, leading to a frequency shift. The frequency shift caused by mass loading can be expressed by Eq. (2)[37,51]:

$$\triangle f = -\frac{f_0}{2m}\triangle m \quad (2)$$

Where $\triangle f$ is the frequency shift, f_0 is the resonance frequency, and $\triangle m$ is the change of mass loading on the prongs. Therefore, there is a negative resonant frequency shift after sensing material coating on the MQTF prongs (Fig. 1b and Supplementary Table 1). When gas is adsorbed onto or desorbed from the sensing material coated on the prongs, the mass loading on the prongs changes, leading to a frequency shift. Although the adsorption kinetics of different gases and sensing materials vary, gas concentration influences the quantity of the adsorbed gas, causing a change in mass loading on the prongs. Since the mass change is linearly correlated with frequency shift, the frequency shift can be used to determine the gas concentration. Theoretical calculations suggest that the mass sensitivity of MQTF can reach 1.3 ng mass loading per 1 Hz frequency shift and further enhancement of mass sensitivity is achievable by improving the frequency accuracy of MQTF[37]. A finite element model simulation reveals that the frequency shift increases linearly with the mass loading on MQTF within a suitable range, but a high added mass may induce some non-linear behavior[52].

Gaseous species with a stronger affinity to the sensing material result in higher gas adsorption. The sensitivity and selectivity can be tuned by changing the gas and sensing material interaction. MXene has a high surface-to-volume ratio, which is beneficial to sensor sensitivity when used as a sensing material. By modifying the functional groups of MXene, the interaction between gases and MXene changes. Therefore, the selectivity and sensitivity can be tuned. Alkaline gas (NH_3), acidic gas (SO_2), and neutral gas (CO) are the three most representative gases in the environment. To selectively detect CO, NH_3, and SO_2, the MXene surface was modified with -F and -NH_2 groups.

MXene synthesis, surface modification, and characterization

Figure 2a shows the preparation process of surface functionalized $Ti_3C_2T_x$ sheets. Firstly, the $Ti_3C_2T_x$ (Supplementary Fig. 7) sheets were fabricated by selectively etching the Al atom of Ti_3AlC_2 particles using LiF/HCl aqueous solution[53]. The obtained $Ti_3C_2T_x$ sheets possess an abundance of terminal groups where Tx denotes the surface terminations on the Ti_3C_2 sheet, including hydroxyl (-OH), oxygen (-O), and fluorine (-F). These terminal groups provide enough active sites for modification or surface engineering to improve selective interaction for target gases or increase hydrophobic performance. Herein, two representative chemical agents, 1H,1H,2H,2H-perfluorooctcyltrithoxysilane (FOTS) and [3-(2-aminoethylamino)propyl] trimethoxysilane (AEAPTMS) (Supplementary Fig. 8), were used to modify the $Ti_3C_2T_x$ sheets, denoted as $Ti_3C_2T_x$-F and $Ti_3C_2T_x$-NH_2, respectively. FOTS was selected because it could bring hydrophobicity to pristine MXene through surface chemistry and enhance the overall performance of the MXene-based chemical sensors[54,55]. Through hydrolysis, FOTS transforms Si–OCH_2CH_3 groups into Si–OH groups and forms covalent bonds (Si–O) with $Ti_3C_2T_x$ by reacting with −OH surface termination groups[55]. FOTS functionalization increases the interlayer distance, facilitating gas diffusion and enhancing gas sensing[55]. The FOTS protection layer can also minimize the oxidation tendency of pristine MXenes, stabilizing sensor performance[55]. Moreover, FOTS-functionalized $Ti_3C_2T_x$ exhibits good stability in humid, acidic, and basic environments[55]. AEAPTMS can be chemically grafted onto the surface of $Ti_3C_2T_x$ through covalent bonding between the silanol group and the –OH groups of $Ti_3C_2T_x$[54,56]. AEAPTMS-$Ti_3C_2T_x$ maintains pH responsiveness due to its free amine groups, akin to hydroxyl groups[56]. The existence of available free amine groups on the surface of AEAPTMS- $Ti_3C_2T_x$ for subsequent reactions allows for the selective engineering of MXene-based gas sensors. For instance, AEAPTMS-$Ti_3C_2T_x$ may exhibit a high affinity for acidic gas molecules like SO_2. The detailed preparation procedure for MXene functionalization is given in the Experimental section. The X-ray diffraction (XRD) measurements were conducted to determine the crystal structure of Ti_2AlC_3, $Ti_3C_2T_x$, $Ti_3C_2T_x$-NH_2, and $Ti_3C_2T_x$-F samples in the scan range 10–65°. The XRD patterns of Ti_3AlC_2 in Fig. 2b show a crystalline nature with a

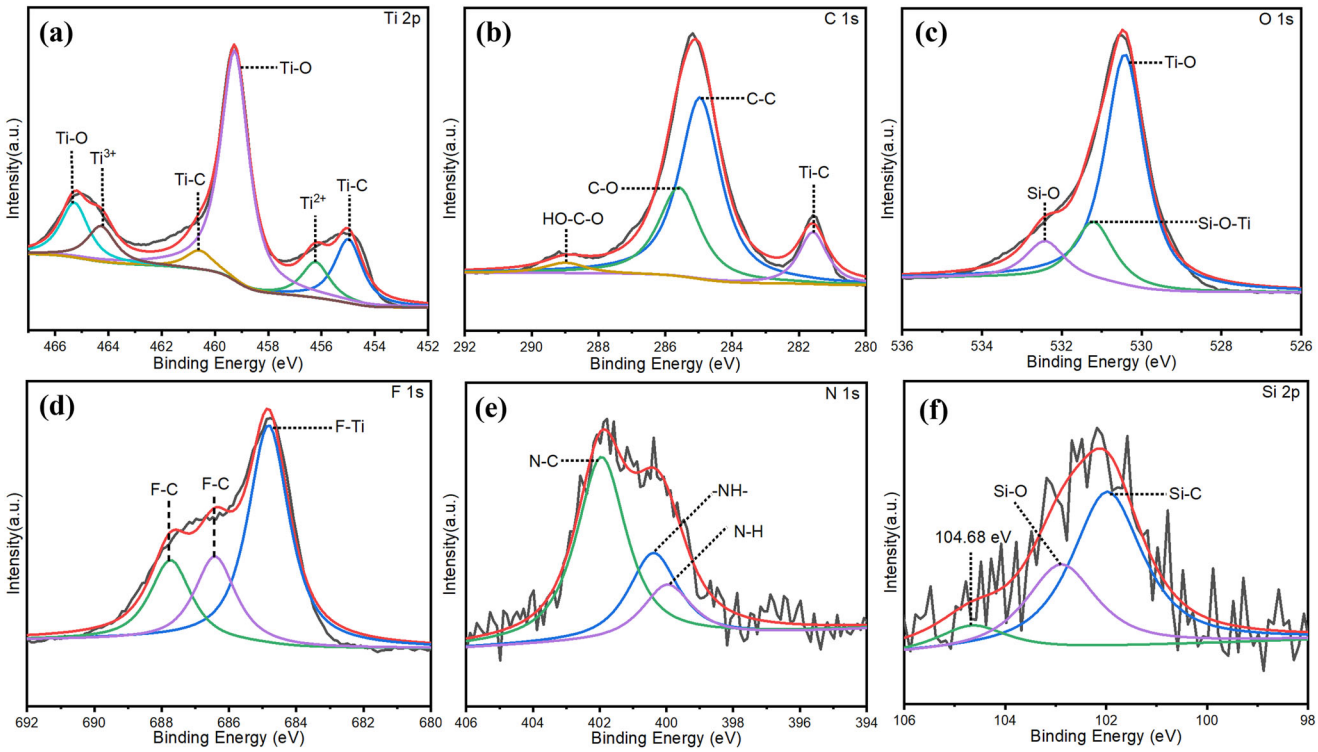

Fig. 3 | XPS spectra of $Ti_3C_2T_x$-NH_2 powders. a–f High-resolution spectra of Ti 2p, C 1 s, O 1 s, F 1 s, N 1 s, and Si 2p, respectively.

preferred orientation along the (104) plane[57]. After HCl/LiF etching, the prominent peak (104) became weaker, and other peaks (101, 102, 103, 105) also became weaker and broader or disappeared. These observations indicate that Al layers were appropriately removed from Ti_3AlC_2, and $Ti_3C_2T_x$ was formed[58].

Scanning electron microscopy (SEM) images of Ti_3AlC_2 and as-etched $Ti_3C_2T_x$-NH_2, as shown in Fig. 1c-d, and Supplementary Fig. 4a-d, clearly reveal a successful transition from a bulk Ti_3AlC_2 to a loosely stacked $Ti_3C_2T_x$ structure after the selective etching process. We also performed the energy dispersive X-ray spectroscopy (EDS) mappings of $Ti_3C_2T_x$-NH_2 (Fig. 1e). The results show a uniform distribution of Ti, C, Si, and N elements within the sheet, suggesting a homogeneous functionalization of $Ti_3C_2T_x$ after AEAPTMS modification.

The elemental composition and surface functional groups were shown by X-ray photoelectron spectroscopy (XPS) (Fig. 3, Supplementary Fig. 5, and 6, Table 4). The XPS measurements were performed on the MXene powders to analyze the type and relative amount of surface functionalities. Figure 3 depicts the XPS spectra of $Ti_3C_2T_x$-NH_2 powders. The XPS spectra $Ti_3C_2T_x$ and $Ti_3C_2T_x$-F powders are shown in Supplementary Fig. 5 and 6. The $Ti_3C_2T_x$-NH_2 sample showed the presence of Ti, C, O, F, N, and Si elements, respectively. In the Ti 2p region (Fig. 3a), there are six peaks corresponding to Ti-O, Ti^{3+}, Ti-C, Ti-O, Ti^{2+}, and Ti-C, at 465.28 eV, 464.28 eV, 460.58 eV, 459.28 eV, 456.18 eV, and 455.08 eV[59], respectively. The Ti-O (465.28 eV) peak is attributed to the anatase titania signals due to the partial oxidation of $Ti_3C_2T_x$-NH_2 MXenes during the synthesis process. The C 1 s region (Fig. 3b) was fitted with five different peaks corresponding to HO-C-O, C-O, C-C, and Ti-C at 288.98 eV, 285.58 eV, 284.44 eV, and 281.58 eV[60], respectively. For the O 1 s core level (Fig. 3c), there are three fitting peaks corresponding to Si-O, Si-O-Ti, and Ti-O on the MXene surface, at 532.48 eV, 531.18 eV, and 530.38 eV, respectively[61]. The Si-O and Si-O-Ti peaks prove that the surface terminal groups in $Ti_3C_2T_x$ react with the polar $Si(OCH_3)_3$ groups in AEAPTMS molecules, forming covalent bonds. The F 1 s core level (Fig. 3d) also could be split into three main peaks of F-C, F-C, and F-Ti, located at 687.68 eV, 686.48 eV, and 684.88 eV, respectively[62]. The N 1 s (Fig. 3e) was deconvoluted into N-C (401.98 eV), -NH- (400.38 eV), and N-H (400.08 eV)[63]. The Si 2p spectra (Fig. 3f) presented three peaks related to 104.66 eV, Si-O (102.88 eV), and Si-C (101.98 eV)[64]. Combined with the previous element analysis in Fig. 2e, surface elements and core elements were uniformly distributed across MXene powder. The N-H functional group on the MXene surface was also confirmed by FTIR analysis (see Supplementary Fig. 13). These results suggest that -F, -OH, and -NH_2 terminal groups appeared on the surface of $Ti_3C_2T_x$-NH_2 flakes. In addition, the F/Ti weight ratio of $Ti_3C_2T_x$-F (27.75%) is obviously larger than that of $Ti_3C_2T_x$ (22.43%), indicating there are more fluorine terminal groups on the surface of $Ti_3C_2T_x$-F.

Characteristics of the MXene-MQTF sensor

The sensors were exposed to different gases to evaluate the essential characteristics of the MXene-MQTF sensors. The sensor responses were recorded with a homemade frequency monitoring device. The typical gas response curves are shown in Fig. 4a with the $Ti_3C_2T_x$-NH_2 MXene sensor exposed to sulfur dioxide at 100 ppm. The sensor was stable under air exposure. When the sensor is exposed to the target gas, it responds quickly and finally reaches a plateau because of adsorption kinetics. The sensor response will return to baseline after air exposure, which means the sensor is reversible. The response and recovery times of $Ti_3C_2T_x$-NH_2 are about 112 s and 153 s, respectively. Here, the response time ($\tau_{response}$) was defined as the time taken for the sensor frequency to achieve 90% of the saturated frequency change. Similarly, the recovery time ($\tau_{recovery}$) is when the sensor returns to 10% of the saturated frequency change after air exposure. The response/recover time of our sensor is comparable with other reported MXene-based gas sensors (Supplementary Table 5). The sensor's response time is influenced by various factors, including the affinity between the gas analyte and MXene, the gas delivery system's flow rate, and the detection chamber's dead space. We anticipate that the response/recovery time of our MXene-MQTF sensor can be further decreased by increasing the sample flow rate and reducing the dead space of the detection chamber. To evaluate the repeatability of the MXene-MQTF sensor, the sensor was exposed to air and 100 ppm SO_2 alternately, as shown in Fig. 4b. The results indicate that the sensor has good repeatability. Therefore, these results demonstrated the

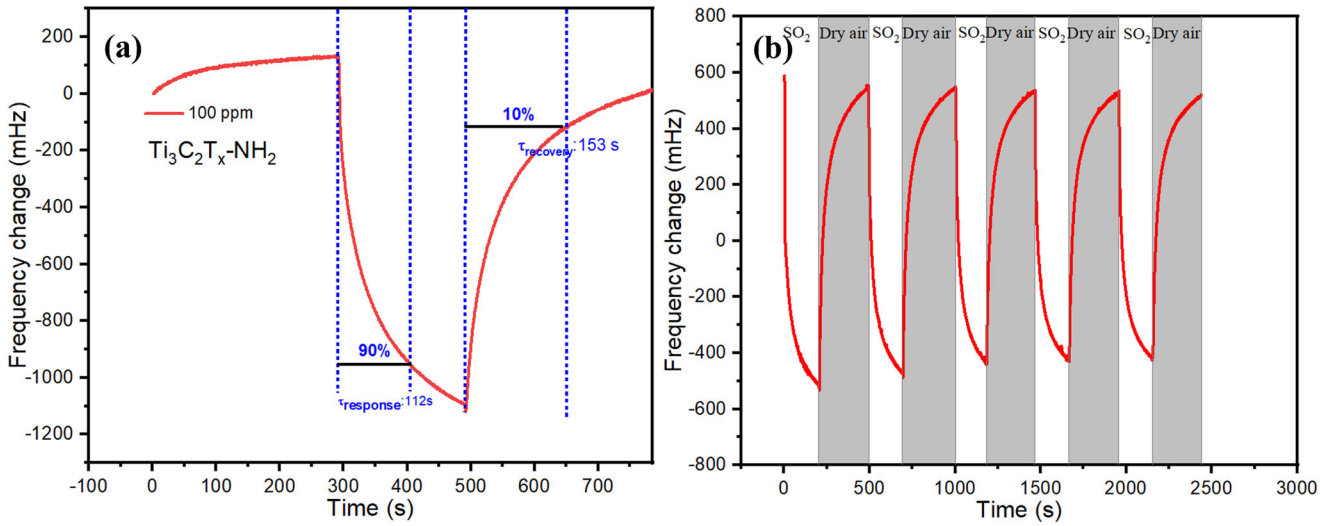

Fig. 4 | Sensing characteristics of $Ti_3C_2T_x$-NH_2-25 MXene sensors. a Response and recovery time calculated for 100 ppm of SO_2. **b** Cycling performance of $Ti_3C_2T_x$-NH_2 MXene Sensors in response to SO_2 at 100 ppm level.

ability of the MXene gas sensor to detect SO_2 gas with good reversibility and repeatability. Moreover, the sensitivity of the MXene-MQTF sensor remained stable, showing less than a 10% change over three weeks (see Supplementary Fig. 12).

Modulating sensor selectivity through surface-modification of MXenes

To compare the sensitivity of $Ti_3C_2T_x$, $Ti_3C_2T_x$-NH_2, and $Ti_3C_2T_x$-F MXene Sensors toward different gases, sensors were exposed to three different gases (CO, SO_2, and NH_3) at a wide range of concentrations (4–100 ppm) as shown in Fig. 5. Figure 5a–i show the real-time gas response of $Ti_3C_2T_x$, $Ti_3C_2T_x$-NH_2, and $Ti_3C_2T_x$-F MXene Sensors under exposure to CO, SO_2, and NH_3 at different concentrations at room temperature. Three repeated cycles were tested for each concentration. All sensors for different gases showed good reversibility. The sensors' responses to different gases were calculated, and the calibration plots of the frequency change versus concentration were plotted in Fig. 5j, k. The error bars in Fig. 5j, k were calculated from three repeated cycles at each concentration. The results showed small error bars for all sensors indicating good sensor repeatability.

The calibration plots were linearly fitted to compare the sensors' sensitivities and selectivities. The slope of the linear fitting curve indicates the sensors' sensitivities. Figure 6a shows the sensitivities and selectivities of the different sensors for different gases. The slopes of $Ti_3C_2T_x$, $Ti_3C_2T_x$-NH_2-60, and $Ti_3C_2T_x$-F MXene Sensors toward SO_2 gas are 5.71, 11.18, and 4.68 (Supplementary Table 2), respectively. Compared to $Ti_3C_2T_x$ and $Ti_3C_2T_x$-F MXene Sensors, the $Ti_3C_2T_x$-NH_2 MXene sensor had the highest response to SO_2 gas. According to XPS and EDS analyses, –NH_2 functional groups were present on the surface of $Ti_3C_2T_x$-NH_2, which reacted with the SO_2 gases. Therefore, $Ti_3C_2T_x$-NH_2 MXene is a promising gas-sensing material for detecting SO_2. $Ti_3C_2T_x$-F MXene Sensor had the strongest response to CO gas, compared to the other two MXene sensors. The FOTS molecules with fluorine ended-groups were covalently bonded onto the surface of $Ti_3C_2T_x$ MXene, which was demonstrated to improve CO gas absorption.

The surface functionalization of $Ti_3C_2T_x$ with AEAPTMS brings free amine groups to the MXene surface. These free amine groups show pH responsiveness, similar to hydroxyl groups[56]. Since SO_2 is acidic, when exposed to SO_2, a donor−acceptor chemistry between SO_2 and amine groups will happen[65]. Using functionalized amine groups to reversibly attract SO_2 has been commonly used to design SO_2 absorbents or sensors[66,67]. The $Ti_3C_2T_x$-NH_2 MXene sensors were decorated with alkaline -NH_2 groups, which promotes the reaction between $Ti_3C_2T_x$-NH_2 MXene and the acidic gas (SO_2) (Fig. 6b). Therefore, the highest sensitivity to SO_2 gas on the $Ti_3C_2T_x$-NH_2 MXene sensors is expected. On the other hand, the lower sensitivity for NH_3 was due to the weaker hydrogen bond between NH_3 gas and the amino functional groups on the surface of $Ti_3C_2T_x$-NH_2 MXene[68]. In addition, CO is a neutral gas and was adsorbed by the surface group of $Ti_3C_2T_x$-NH_2 MXene through Van der Waals forces. Since the Van der Waals force interaction is weak and non-specific, the sensitivity of $Ti_3C_2T_x$-NH_2 MXene to CO is very low. FOTS functionalization brings C-F groups to the pristine MXene through surface chemistry. This modification improves MXene's hydrophobicity and stability in humid, acidic, and basic environments, attributed to the high stability of fluoro-carbon bonds. Studies indicate that $Ti_3C_2T_x$-F films maintain contact angles over 150° even after exposure to deionized water, strongly acidic, or basic solutions[55]. This implies weak interactions of $Ti_3C_2T_x$-F with acidic, basic, or neutral gases. Our $Ti_3C_2T_x$-F sensor exhibits low and similar sensitivity to SO_2, NH_3, and CO, which is consistent with the literature. Theoretical investigations suggest that the functional groups of MXene can influence the adsorption energy of a gas analyte, and sensitivity enhancement can be achieved through the manipulation of MXene's functional groups[19,69–71]. Our experimental results corroborate these theoretical findings. Research indicates that chemisorption is a dominant process in gas adsorption on MXenes[72], and the elevated selectivity of MXene-based gas sensors is attributed to the existence of surface functional groups[73]. Specifically, the terminal OH-groups on the MXene surface exhibit robust acidic properties and have the potential to adsorb "basic" gases[74]. The selectivity observed in the MXene-MQTF sensor aligns with the findings reported in the literature.

We noticed that the MXene-MQTF sensor exhibited sensitivity to humidity, which was an inherent characteristic of mass transducers due to the adsorption of H_2O on both the sensing material and even the bare MQTF[75]. But the humidity effect followed a linear behavior (Supplementary Fig. 2 and 3) and can be corrected through humidity compensation algorithms. An MQTF reference coated with humidity-sensitive materials, such as silica, can be incorporated into the sensing device alongside the MXene-MQTF sensor. The signal from the reference MQTF can then be subtracted from the MXene-MQTF sensor to eliminate the impact of humidity. Other methods could also mitigate humidity interference, such as using Nafion™ tubing or desiccants[76]. Nafion, a chemically inert copolymer with high water permeability, enables the passage of water molecules through its membrane while preventing analyte gas molecules from permeating. This quality makes it well-suited for regulating the humidity of gas samples. Integrating Nafion tubing at the inlet of the gas sensing chamber proves effective in avoiding humidity interference[77]. To avoid the direct interaction of water molecules with the sensing unit, desiccants can be implemented at the gas

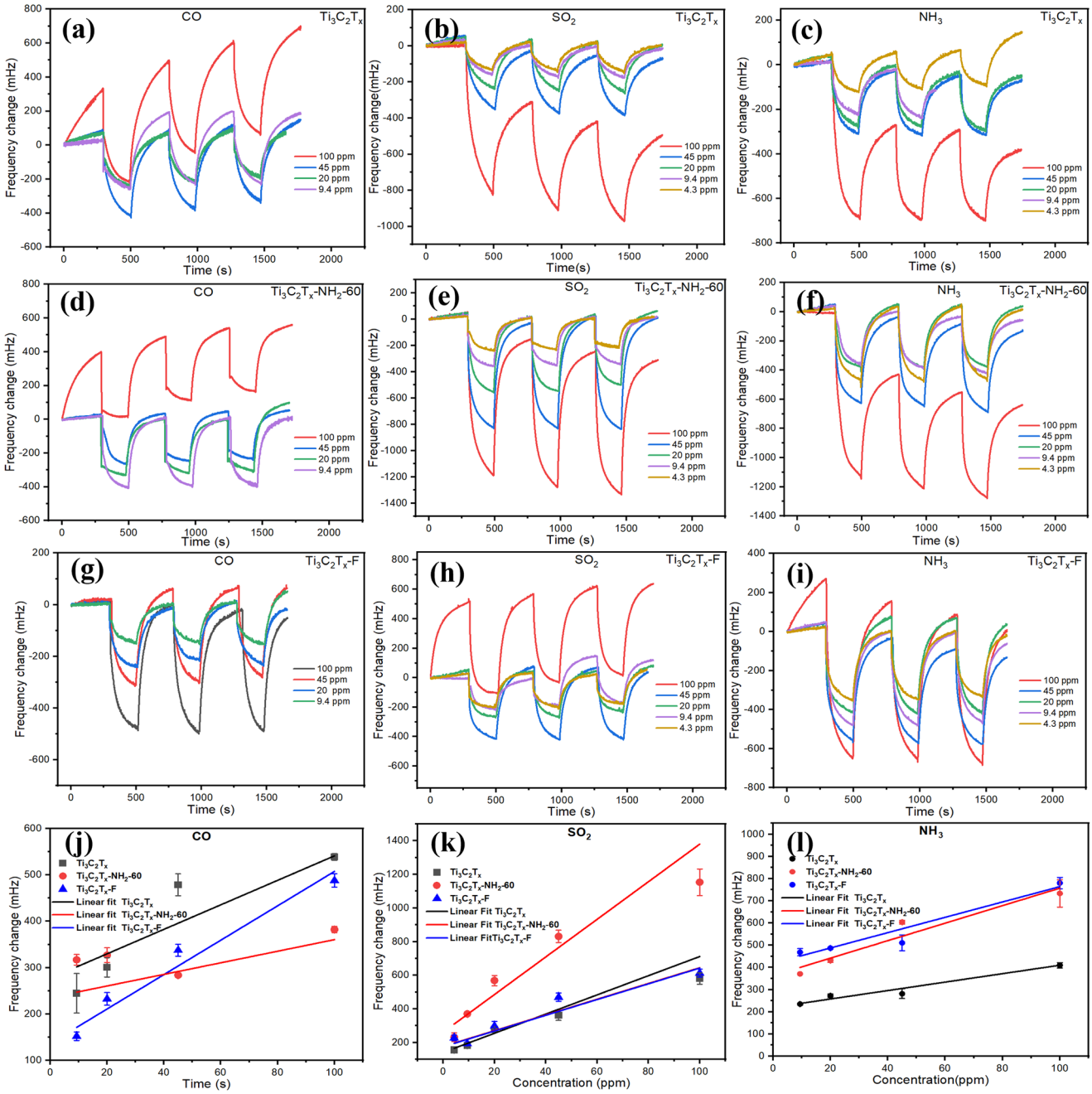

Fig. 5 | Gas response performance of $Ti_3C_2T_x$, $Ti_3C_2T_x$-NH_2, and $Ti_3C_2T_x$-F MXene sensors at room temperature. Frequency change on **a**–**c** $Ti_3C_2T_x$; **d**–**f** $Ti_3C_2T_x$-NH_2; **g**, **h** and **i** $Ti_3C_2T_x$ -F toward a wide range of diluted CO, SO_2, and NH_3 gases (4–100 ppm). **j**–**l** Maximal frequency change and its fitting result in a wide range of diluted CO, SO_2, and NH_3 gases (4 –100 ppm). The error bars are the standard deviation (s.d.) of the measured results of three repeated cycles.

inlet to remove water vapor before delivering the gas sample to the sensing chamber. Desiccants can effectively reduce ambient humidity levels to near zero during gas sample pretreatment[76].

Sensitivity enhancement through surface chemistry

To further improve the response of the $Ti_3C_2T_x$-NH_2 sensors toward SO_2 gas, the temperature during surface modification of the $Ti_3C_2T_x$-NH_2 MXene materials was changed from 25 to 60 °C. The reaction temperature cannot be increased further because a mixture of ethanol and water (90/10 wt%) was used as the solvent. We investigated MXene's morphology change at different reaction temperatures (Supplementary Fig. 11). There were no obvious structure changes on MXenes when the reaction temperature increased from 25 °C to 60 °C. Similar to the above procedures, three cycles for each concentration were tested for different sensing materials prepared at different temperatures. Supplementary Fig. 7 shows the frequency change of the $Ti_3C_2T_x$-NH_2 MXene sensor versus SO_2 gas concentration, ranging from 4.3 to 100 ppm. According to the slope of the fitting results, sensor sensitivity versus material preparation temperature was plotted in Fig. 7d. When the temperature increased from 25 to 60 °C, the sensitivity increased from 6.18 to 11.18, possibly due to more -NH_2 functional groups on the $Ti_3C_2T_x$-NH_2 MXene surface. It's important to note that excessively high reaction temperatures may accelerate the degradation of $Ti_3C_2T_x$ due to dissolved oxygen in water[56,78]. Therefore, there's a trade-off linked to raising the reaction temperature for MXene surface modification.

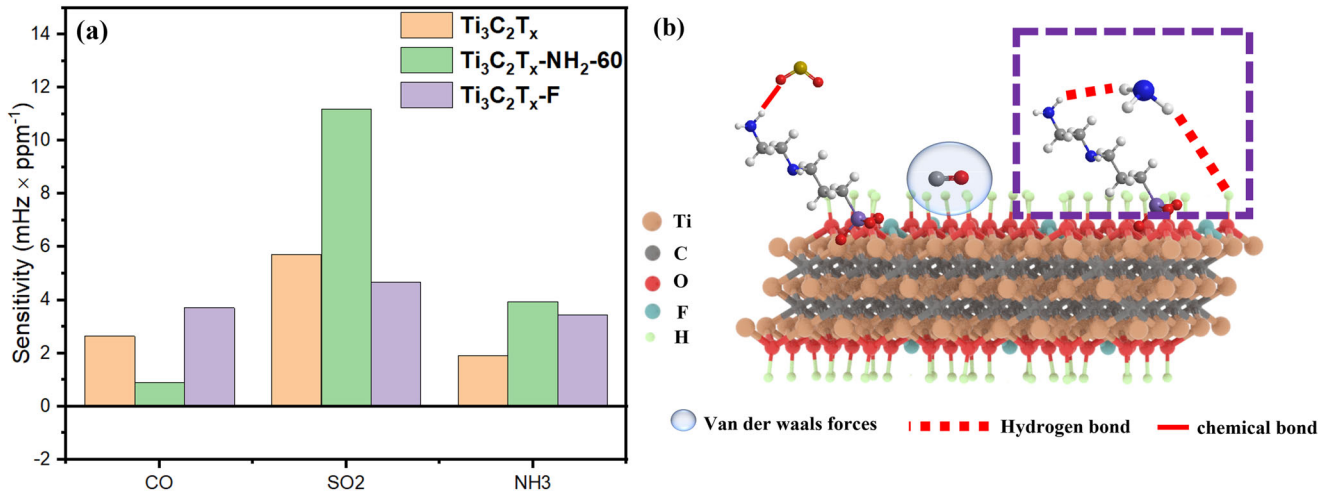

Fig. 6 | Gas response performance of MXene sensors toward three different kinds of gases at room temperature. a Selectivity test of the $Ti_3C_2T_x$, $Ti_3C_2T_x$-NH_2-60, and $Ti_3C_2T_x$ -F sensors upon exposure to ammonia, sulfur dioxide, and carbon monoxide. **b** Schematic illustration of the interaction between $Ti_3C_2T_x$-NH_2 and the related gases (monoxide carbon, sulfur dioxide, and ammonia).

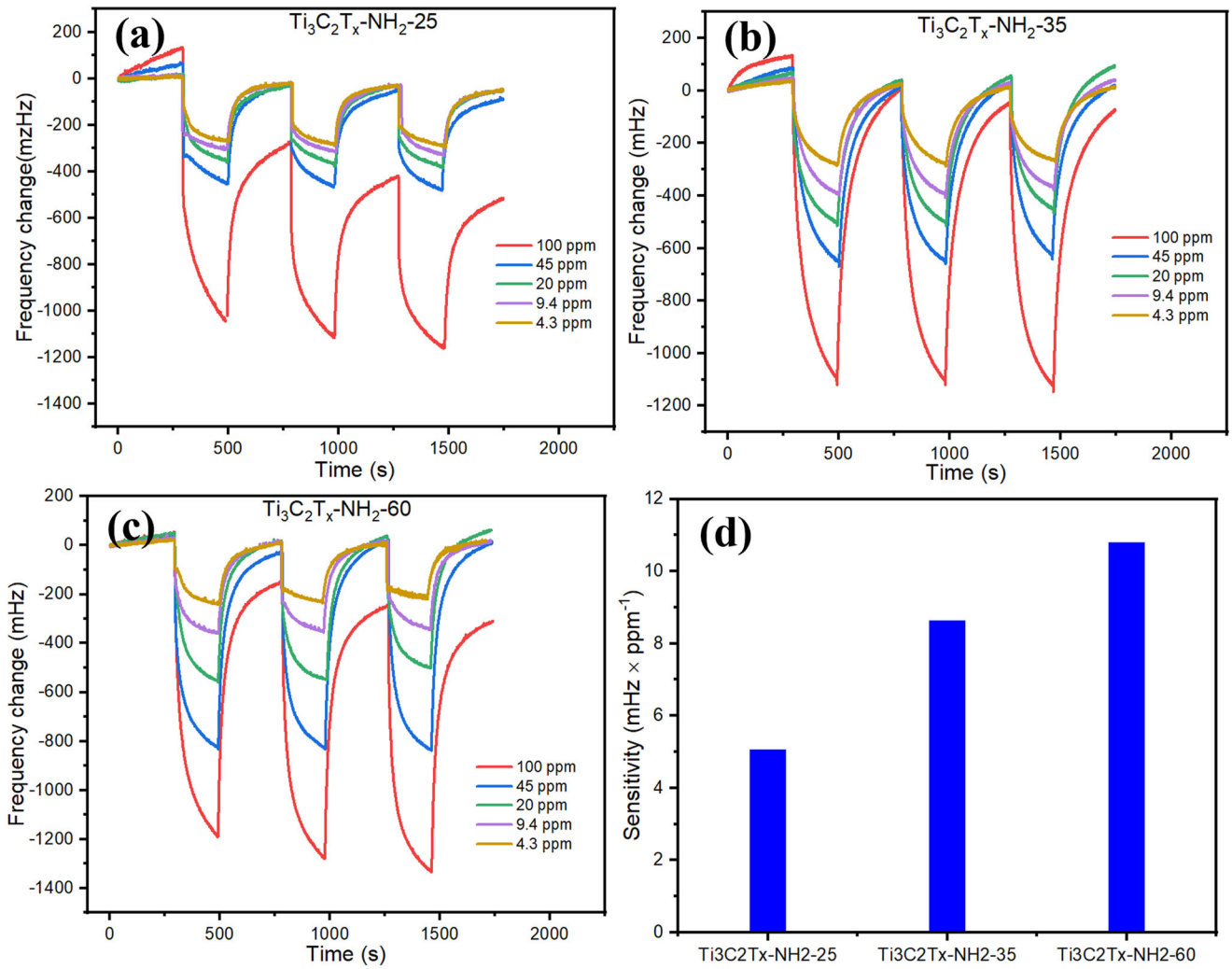

Fig. 7 | Gas response performance of $Ti_3C_2T_x$-NH_2 sensors toward sulfur dioxide gas. Frequency change toward SO_2 at different concentrations for sensors based on $Ti_3C_2T_x$-NH_2 prepared at **a** 25 °C, **b** 35 °C, and **c** 60 °C. **d** sensitivity of the $Ti_3C_2T_x$-NH_2 sensors upon exposure to sulfur dioxide.

In summary, we successfully designed, fabricated, and tested the $Ti_3C_2T_x$-MQTF gas sensors, in which MXenes served as the selective receptors and MQTF as the transducer. The binding of gas molecules to MXenes induced mass change, resulting in MQTF's resonant frequency shift. We synthesized $Ti_3C_2T_x$ and introduced various chemical groups to its surface. By coating the surface-modified $Ti_3C_2T_x$ onto the tips of the MQTF as a recognition layer, we created MXene-MQTF gas sensors capable of sensitive, selective, and reversible detection of CO, SO_2, and NH_3. The test results indicated that surface-functionalized $Ti_3C_2T_x$ exhibited significantly improved gas sensing performance compared to pristine $Ti_3C_2T_x$. $Ti_3C_2T_x$-NH_2-based sensors exhibited high selectivity to SO_2, an acidic gas. In contrast, $Ti_3C_2T_x$-F-based sensors showed the strongest response toward CO. $Ti_3C_2T_x$-NH_2 and $Ti_3C_2T_x$-F were covered with -NH_2 and -F functional groups, respectively, which contributed to the selective detection of the specific gases. Furthermore, the sensitivity and selectivity of $Ti_3C_2T_x$ -MQTF gas sensors can be enhanced by introducing additional surface chemical groups to MXenes by increasing the material preparation temperatures during surface modification reactions. For instance, the sensitivity of the $Ti_3C_2T_x$-NH_2-MQTF sensor for SO_2 detection doubled when the surface modification temperature was increased from 25 to 60 °C. These findings strongly indicate that the sensitivity and selectivity of MXene-MQTF gas sensors can be fine-tuned through surface chemistry engineering of $Ti_3C_2T_x$. This study presented an approach for designing high-performance MXene-based chemical sensors, expanding the potential applications of MXene-based chemical sensors in diverse fields such as air quality monitoring, wearable devices, Internet of Things (IoT), and robotics.

Methods

Materials

Micro quartz tuning forks, purchased from the Jiangcheng Electronic Limited Company, China, have a typical resonant frequency of ~32768 Hz with dimensions of 4 mm × 0.35 mm × 0.6 mm. Ti_3AlC_2 (particle size <100 μm), LiF, HCl (36 ~ 38 wt%), 1H,1H,2H,2H-perfluorooctyltrithoxysilane (FOTS) and [3-(2-aminoethylamino)propyl]trimethoxysilane (AEAPTMS) were purchased from Sigma-Aldrich.

Synthesis of $Ti_3C_2T_x$ MXene

Ti_3AlC_2 powder (3 g, particle size <100 μm) was etched to remove its Al in a premix solution of LiF (3 g) and 9 M HCl (30 ml) and stirred for 24 h at 35 °C. Then, the resulting suspension was washed via centrifugation several times with deionized water and ethanol until the pH value reached ~6. Following washing, the final suspension was vacuum-filtered on membranes, and the obtained sample was dried in a vacuum oven at 60 °C for 24 h.

Surface functionalization of $Ti_3C_2T_x$ MXene ($Ti_3C_2T_x$ -NH_2 and $Ti_3C_2T_x$ -F)

First, 40 ml ethanol was added into 360 ml water to prepare a water/ethanol mixture of 10/90 wt%. Then, 800 mg $Ti_3C_2T_x$ MXene was added into the above solution and stirred at 600 rpm for 10 min with nitrogen bubbling to make the reaction go thoroughly. In addition, acetic acid was added to adjust the pH of the above solution to 3.5. When the pH reached 3.5, AEAPTMS (1.6 g) was added to the above solution. The reaction needed to be stirred for 8 h under nitrogen bubbling. All reaction steps were performed at 25 °C. After completion of the reaction, the above product was washed three times with ethanol by centrifugation at 3500 rpm to remove residual silane coupling agents from AEAPTMS- $Ti_3C_2T_x$ nanosheets. The final suspension was vacuum-filtered on membranes, and the obtained samples were subsequently dried in a vacuum oven at 60 °C for 24 h, resulting in $Ti_3C_2T_x$ -NH_2-25. When the reaction temperatures were changed to 35 and 60 °C, the samples obtained were $Ti_3C_2T_x$ -NH_2-35 and $Ti_3C_2T_x$ -NH_2-60, respectively. The preparation procedure of $Ti_3C_2T_x$ -F was similar to $Ti_3C_2T_x$ -NH_2-25 except that AEAPTMS was replaced with FOTS at 25 °C.

Coating MXenes on the prongs of micro quartz tuning forks

First, the tuning forks were washed three times in ethanol. Then, 40 mg MXene materials were added to 20 ml water, and the solution was stirred for 10 min. 1 ml of the above solution was removed and dropped onto a glass microscope slide. The tips of the tuning forks were dipped into the above solution. Finally, tuning forks with MXene materials was dried in ambient conditions.

Gas-sensing performance measurements

All the gas-sensing tests were performed at room temperature in a homemade gas-sensing system (see Supplementary Fig. 1). Ambient air was used as the purging gas. The target gases were injected into the sensing chamber at the flow rate of 0.55 L min^−1. For each cycle of the gas test, the durations for introducing the target analyte and purging gas were 200 s and 300 s, respectively. Humidity and temperature in the chamber were monitored with a commercial humidity sensor (Sensirion SHT3x_85).

Sensing material characterization

The morphologies of the MXene materials were characterized by scanning electron microscopy (S-4700, FESEM, Hitachi). The XRD was conducted by a Rigaku SmartLab diffractometer. X-ray photoelectron spectroscopy (Thermo VG Scientific Sigma Probe) was used to characterize the chemical information of the Mxene materials. Infrared spectroscopy (FTIR) measurements were done using a Perkin-Elmer system 2000 spectroscope.

Data availability

The authors declare that the data supporting the findings are available within the paper and its supplementary information. The corresponding authors can also provide data upon reasonable request.

Received: 6 October 2023; Accepted: 12 February 2024;
Published online: 06 March 2024

References

1. Aslam, M. K., Niu, Y. & Xu, M. MXenes for non-lithium-ion (Na, K, Ca, Mg, and Al) batteries and supercapacitors. *Adv. Energy Mater.* **11**, 2000681 (2021).
2. Gao, L. et al. MXene/polymer membranes: synthesis, properties, and emerging applications. *Chem. Mater.* **32**, 1703–1747 (2020).
3. Chen, J. et al. Recent progress and advances in the environmental applications of MXene related materials. *Nanoscale* **12**, 3574–3592 (2020).
4. Lu, B. et al. 2D MXene nanomaterials for versatile biomedical applications: current trends and future prospects. *Small* **17**, 2100946 (2021).
5. Lee, E., VahidMohammadi, A., Yoon, Y. S., Beidaghi, M. & Kim, D.-J. Two-dimensional vanadium carbide MXene for gas sensors with ultrahigh sensitivity toward nonpolar gases. *ACS sens.* **4**, 1603–1611 (2019).
6. Pei, Y. et al. Ti3C2TX MXene for sensing applications: recent progress, design principles, and future perspectives. *ACS nano* **15**, 3996–4017 (2021).
7. Chen, Y. et al. Refractive index sensors based on Ti_3C_2Tx MXene fibers. *ACS Appl. Nano Mater.* **3**, 303–311 (2020).
8. Huang, W., Hu, L., Tang, Y., Xie, Z. & Zhang, H. Recent advances in functional 2D MXene-based nanostructures for next-generation devices. *Adv. Funct. Mater.* **30**, 2005223 (2020).
9. Chen, Z. et al. CRISPR-Cas13a-powered electrochemical biosensor for the detection of the L452R mutation in clinical samples of SARS-CoV-2 variants. *J. Nanobiotechnology* **21**, 141 (2023).
10. Zhang, J. et al. Scalable manufacturing of free-standing, strong Ti_3C_2Tx MXene films with outstanding conductivity. *Adv. Mater.* **32**, 2001093 (2020).

11. Zhang, Y., Xia, W., Wu, Y. & Zhang, P. Prediction of MXene based 2D tunable band gap semiconductors: GW quasiparticle calculations. *Nanoscale* **11**, 3993–4000 (2019).
12. Li, S.-N. et al. Environmentally stable, mechanically flexible, self-adhesive, and electrically conductive Ti_3C_2TX MXene hydrogels for wide-temperature strain sensing. *Nano Energy* **90**, 106502 (2021).
13. Chen, Z. et al. Gel polymer electrolyte with MXene to extend cycle lifespan of flexible and rechargeable Zinc–Air batteries. *J. Power Sources* **523**, 231020 (2022).
14. Qian, A., Seo, J. Y., Shi, H., Lee, J. Y. & Chung, C. H. Surface functional groups and electrochemical behavior in dimethyl sulfoxide-delaminated Ti3C2Tx MXene. *ChemSusChem* **11**, 3719–3723 (2018).
15. Dong, H., Sun, J., Liu, X., Jiang, X. & Lu, S. Highly sensitive and stretchable MXene/CNTs/TPU composite strain sensor with bilayer conductive structure for human motion detection. *ACS Appl. Mater. Interfaces* **14**, 15504–15516 (2022).
16. Lei, D. et al. Roles of MXene in pressure sensing: Preparation, composite structure design, and mechanism. *Adv. Mater.* **34**, 2110608 (2022).
17. Lu, D., Zhao, H., Zhang, X., Chen, Y. & Feng, L. New horizons for MXenes in biosensing applications. *Biosensors* **12**, 820 (2022).
18. Bhardwaj, R. & Hazra, A. MXene-based gas sensors. *J. Mater. Chem. C* **9**, 15735–15754 (2021).
19. Kim, S. J. et al. Metallic Ti3C2T x MXene gas sensors with ultrahigh signal-to-noise ratio. *ACS Nano* **12**, 986–993 (2018).
20. Lee, S. H. et al. Room-temperature, highly durable Ti_3C_2T x MXene/graphene hybrid fibers for NH3 gas sensing. *ACS Appl. Mater. interfaces* **12**, 10434–10442 (2020).
21. Sun, S. et al. W18O49/Ti3C2Tx Mxene nanocomposites for highly sensitive acetone gas sensor with low detection limit. *Sens. Actuators B Chem.* **304**, 127274 (2020).
22. Yang, J. et al. Molecular interaction and inhibition of SARS-$CoV-_2$ binding to the ACE2 receptor. *Nat. Commun.* **11**, 4541 (2020).
23. Yuan, W., Yang, K., Peng, H., Li, F. & Yin, F. A flexible VOCs sensor based on a 3D Mxene framework with a high sensing performance. *J. Mater. Chem. A* **6**, 18116–18124 (2018).
24. Li, N. et al. A fully inkjet-printed transparent humidity sensor based on a Ti_3C_2/Ag hybrid for touchless sensing of finger motion. *Nanoscale* **11**, 21522–21531 (2019).
25. Rasheed, P. A., Pandey, R. P., Rasool, K. & Mahmoud, K. A. Ultra-sensitive electrocatalytic detection of bromate in drinking water based on Nafion/Ti3C2Tx (MXene) modified glassy carbon electrode. *Sens. Actuators B Chem.* **265**, 652–659 (2018).
26. Wu, L. et al. 2D transition metal carbide MXene as a robust biosensing platform for enzyme immobilization and ultrasensitive detection of phenol. *Biosens. Bioelectron.* **107**, 69–75 (2018).
27. Zheng, J. et al. An inkjet printed Ti_3C_2-GO electrode for the electrochemical sensing of hydrogen peroxide. *J. Electrochem. Soc.* **165**, B227 (2018).
28. Cai, Y. et al. Stretchable Ti_3C_2T x MXene/carbon nanotube composite based strain sensor with ultrahigh sensitivity and tunable sensing range. *ACS Nano* **12**, 56–62 (2018).
29. Ma, Y. et al. A highly flexible and sensitive piezoresistive sensor based on MXene with greatly changed interlayer distances. *Nat. Commun.* **8**, 1207 (2017).
30. Ma, Y. et al. 3D synergistical MXene/reduced graphene oxide aerogel for a piezoresistive sensor. *ACS nano* **12**, 3209–3216 (2018).
31. Kaleli-Can, G., Özgüzar, H. F. & Mutlu, M. Development of mass sensitive sensor platform based on plasma polymerization technique: Quartz tuning fork as transducer. *Appl. Surf. Sci.* **540**, 148360 (2021).
32. Giessibl, F. J., Pielmeier, F., Eguchi, T., An, T. & Hasegawa, Y. Comparison of force sensors for atomic force microscopy based on quartz tuning forks and length-extensional resonators. *Phys. Rev. B* **84**, 125409 (2011).
33. Ooe, H., Sakuishi, T., Nogami, M., Tomitori, M. & Arai, T. Resonance frequency-retuned quartz tuning fork as a force sensor for noncontact atomic force microscopy. *Appl. Phys. Lett.* **105**, 043107 (2014).
34. Qin, X. et al. Micro quartz tuning fork-based PM 2.5 sensor for personal exposure monitoring. *IEEE Sens. J.* **19**, 2482–2489 (2018).
35. Tsow, F. et al. A wearable and wireless sensor system for real-time monitoring of toxic environmental volatile organic compounds. *IEEE Sens. J.* **9**, 1734–1740 (2009).
36. Deng, Y. et al. A novel wireless wearable volatile organic compound (VOC) monitoring device with disposable sensors. *Sensors* **16**, 2060 (2016).
37. Zhang, J. & O'shea, S. Tuning forks as micromechanical mass sensitive sensors for bio-or liquid detection. *Sens. Actuators B Chem.* **94**, 65–72 (2003).
38. Xu, L., Liu, K., Liang, J., Li, J. & Zhou, S. Micro-quartz crystal tuning fork-based photodetector array for trace gas detection. *Anal. Chem.* **95**, 6955–6961 (2023).
39. Patimisco, P. et al. Analysis of the electro-elastic properties of custom quartz tuning forks for optoacoustic gas sensing. *Sens. Actuators B Chem.* **227**, 539–546 (2016).
40. Su, X., Dai, C., Zhang, J. & O'Shea, S. J. Quartz tuning fork biosensor. *Biosens. Bioelectron.* **17**, 111–117 (2002).
41. Yamazoe, N. Toward innovations of gas sensor technology. *Sens. Actuators B Chem.* **108**, 2–14 (2005).
42. Eersels, K., Lieberzeit, P. & Wagner, P. A review on synthetic receptors for bioparticle detection created by surface-imprinting techniques from principles to applications. *ACS sens.* **1**, 1171–1187 (2016).
43. Postolache, O. A., Pereira, J. D. & Girao, P. S. Smart sensors network for air quality monitoring applications. *IEEE Trans. Instrum. Meas.* **58**, 3253–3262 (2009).
44. Rossi, M. et al. Gas-Drone: portable gas sensing system on UAVs for gas leakage localization. In *SENSORS, 2014 IEEE,* 1431–1434 (IEEE, 2014).
45. Jia, Q. et al. Rapid and selective detection of acetone using hierarchical ZnO gas sensor for hazardous odor markers application. *J. Hazard. Mater.* **276**, 262–270 (2014).
46. Kampa, M. & Castanas, E. Human health effects of air pollution. *Environ. Pollut.* **151**, 362–367 (2008).
47. Kong, L. et al. Evaluation and uncertainty investigation of the NO_2, CO and NH_3 modeling over China under the framework of MICS-Asia III. *Atmos. Chem. Phys.* **20**, 181–202 (2020).
48. Zhang, T., Liu, L., Qi, Q., Li, S. & Lu, G. Development of microstructure In/Pd-doped SnO_2 sensor for low-level CO detection. *Sens. Actuators B Chem.* **139**, 287–291 (2009).
49. Salih, E. & Ayesh, A. I. CO, CO_2, and SO_2 detection based on functionalized graphene nanoribbons: First principles study. *Physica E Low Dimens. Syst. Nanostruct.* **123**, 114220 (2020).
50. Wu, M. et al. Ti3C2 MXene-based sensors with high selectivity for NH3 detection at room temperature. *ACS Sens.* **4**, 2763–2770 (2019).
51. Zhou, S. et al. Absorption spectroscopy gas sensor using a low-cost quartz crystal tuning fork with an ultrathin iron doped cobaltous oxide coating. *Sens. Actuators B Chem.* **326**, 128951 (2021).
52. Oria, R. et al. Finite element analysis of electrically excited quartz tuning fork devices. *Sensors* **13**, 7156–7169 (2013).
53. Shi, H. et al. Ambient-stable two-dimensional titanium carbide (MXene) enabled by iodine etching. *Angew. Chem. Int. Ed.* **60**, 8689–8693 (2021).
54. Mozafari, M. & Soroush, M. Surface functionalization of MXenes. *Mater. Adv.* **2**, 7277–7307 (2021).
55. Chen, W. Y. et al. Surface functionalization of Ti_3C_2Tx MXene with highly reliable superhydrophobic protection for volatile organic compounds sensing. *ACS Nano* **14**, 11490–11501 (2020).
56. Riazi, H. et al. Surface modification of a MXene by an aminosilane coupling agent. *Adv. Mater. Interfaces* **7**, 1902008 (2020).
57. Quispe, R. et al. Tribological and mechanical performance of Ti_2AlC and Ti_3AlC_2 thin films. *Adv. Eng. Mater.* **24**, 2200188 (2022).

58. Ashok, A., Saseendran, S. B. & Asha, A. Synthesis of Ti_3C_2Tx MXene from the Ti_3AlC_2 MAX phase with enhanced optical and morphological properties by using ammonia solution with the in-situ HF forming method. *Phys. Scr.* **97**, 025807 (2022).
59. Natu, V. et al. A critical analysis of the X-ray photoelectron spectra of Ti_3C_2Tz MXenes. *Matter* **4**, 1224–1251 (2021).
60. Pang, J. et al. Applications of 2D MXenes in energy conversion and storage systems. *Chem. Soc. Rev.* **48**, 72–133 (2019).
61. Hou, T. et al. Modulating oxygen coverage of Ti_3C_2Tx MXenes to boost catalytic activity for HCOOH dehydrogenation. *Nat. Commun.* **11**, 4251 (2020).
62. Zhou, Y., Wang, Y., Wang, Y. & Li, X. Humidity-enabled ionic conductive trace carbon dioxide sensing of nitrogen-doped Ti_3C_2T x MXene/polyethyleneimine composite films decorated with reduced graphene oxide nanosheets. *Anal. Chem.* **92**, 16033–16042 (2020).
63. Zhang, W.-J. et al. Dual (pH-and ROS-) Responsive antibacterial mxene-based nanocarrier for drug delivery. *Int. J. Mol. Sci.* **23**, 14925 (2022).
64. Kong, F. et al. Enhanced reversible Li-ion storage in Si@ Ti_3C_2 MXene nanocomposite. *Electrochem. Commun.* **97**, 16–21 (2018).
65. Leontiev, A. V. & Rudkevich, D. M. Revisiting noncovalent SO_2- amine chemistry: an indicator− displacement assay for colorimetric detection of SO_2. *J. Am. Chem. Soc.* **127**, 14126–14127 (2005).
66. Hong, S. Y. et al. Nitrile-functionalized tertiary amines as highly efficient and reversible SO_2 absorbents. *J. Hazard. Mater.* **264**, 136–143 (2014).
67. Matsuguchi, M., Tamai, K. & Sakai, Y. SO_2 gas sensors using polymers with different amino groups. *Sens. Actuators B. Chem.* **77**, 363–367 (2001).
68. Khakbaz, P. et al. Titanium carbide MXene as NH_3 sensor: realistic first-principles study. *J. Phys. Chem. C* **123**, 29794–29803 (2019).
69. Hajian, S. et al. Impact of different ratios of fluorine, oxygen, and hydroxyl surface terminations on Ti3C2T x MXene as ammonia sensor: a first-principle study. In *2018 IEEE SENSORS*, 1–4 (IEEE, 2018).
70. Ma, S., Yuan, D., Jiao, Z., Wang, T. & Dai, X. Monolayer Sc_2CO_2: a promising candidate as a SO_2 gas sensor or capturer. *J. Phys. Chem. C* **121**, 24077–24084 (2017).
71. Yang, D. et al. Sc_2CO_2 and Mn-doped Sc_2CO_2 as gas sensor materials to NO and CO: A first-principles study. *Physica E Low Dimens. Syst. Nanostruct.* **111**, 84–90 (2019).
72. Junkaew, A. & Arroyave, R. Enhancement of the selectivity of MXenes (M_2C, M= Ti, V, Nb, Mo) via oxygen-functionalization: promising materials for gas-sensing and-separation. *Phys. Chem. Chem. Phys.* **20**, 6073–6082 (2018).
73. Xia, Q. et al. MXene-based chemical gas sensors: Recent developments and challenges. *Diam. Relate. Mater.* **131**, 109557 (2023).
74. Petukhov, D. et al. MXene-based gas separation membranes with sorption type selectivity. *J. Memb. Sci.* **621**, 118994 (2021).
75. Kim, W., Park, E. & Jeon, S. Performance enhancement of a quartz tuning fork sensor using a cellulose nanocrystal-reinforced nanoporous polymer fiber. *Sensors* **20**, 437 (2020).
76. Yu, J., Wang, D., Tipparaju, V. V., Tsow, F. & Xian, X. Mitigation of humidity interference in colorimetric sensing of gases. *ACS Sens.* **6**, 303–320 (2020).
77. Prabhakar, A. et al. Ultrasensitive detection of nitrogen oxides over a nanoporous membrane. *Anal. Chem.* **82**, 9938–9940 (2010).
78. Zhang, C. J. et al. Oxidation stability of colloidal two-dimensional titanium carbides (MXenes). *Chem. Mater.* **29**, 4848–4856 (2017).

Acknowledgements

The authors thank the startup fund from the Department of Electrical Engineering and Computer Science at South Dakota State University and the SDSU-RSCA F24 fund for supporting this research.

Author contributions

W.D. and J.Y. contributed equally to this work. X.X. conceived the project, directed the research and experiments, and raised the funding. W.D. synthesized the MXenes, and performed materials characterization, sensor fabrication and testing, and data analysis. J.Y. designed, synthesized and characterized the MXenes, built the circuit for frequency reading, and fabricated the sensor testing setup. F.T. designed the circuit and contributed to tuning fork sensor development. L.J. helped with the testing setup improvement. R.K. helped with the circuit improvement. B.S.L., S.A., and Y.Z. helped with the materials characterization. P.K. helped with the XRD test. W.D. and X.X. co-wrote the manuscript with input from all authors.

Competing interests

The authors declare no competing interests.

Additional information

Supplementary information The online version contains supplementary material available at https://doi.org/10.1038/s41699-024-00452-1.

Correspondence and requests for materials should be addressed to Xiaojun Xian.